1 Introduction

The aspiration to fly faster and higher has always been the driving force behind the progress of aeronautics. This desire stems from the practical need for faster modes of transportation as well as humanity's innate curiosity to explore the unknown. To travel to new worlds, humans or their devices must transcend the confines of this planet.

Hypersonic flight not only draws the imagination of space travel to exotic realms and peaceful exploration of space but also evokes dire portents of military exploitation. Machines that are developed to fly at hypersonic speeds must first be tested on the ground in order to evaluate their designs. This book is about ground testing of hypersonic flight vehicles. We will define more precisely what hypersonic means later in the chapter but suffice here to say that it refers to flight at velocities much greater than the speed of sound. Because of the high speeds encountered, hypersonic flight involves extreme flow conditions that are very difficult to replicate in ground testing facilities.

Hypersonic flight occurs when a missile, rocket, aircraft, or spacecraft travels through the atmosphere at the extreme high-speed end of the flight spectrum. This can occur when an intercontinental ballistic missile reenters Earth's atmosphere. A similar situation occurs when a spacecraft reenters Earth's atmosphere from a low Earth orbit (LEO) or when it returns from the Moon or other celestial bodies in the solar system.

For Earth-orbiting spacecraft, the reentry into Earth's atmosphere poses a major challenge. The orbital velocity of LEO spacecraft is approximately 7.5 km/s (or Mach 25). When the spacecraft reenters the atmosphere at this speed, the shock-heated gas around the vehicle results in high heating on the vehicle's surface. Therefore, it is vital to design the thermal protection system (TPS) for the vehicle's survival during reentry. However, there is little room for safety factors and conservative designs, as these spacecraft have very stringent weight requirements. A conservative TPS design would mean that the heat shield is too massive for any payload to be carried.

Spacecraft returning from Moon missions will reenter Earth's atmosphere at higher velocities than those from LEOs. The Apollo command modules that carried the returning astronauts from the Moon reentered Earth's atmosphere at approximately 11 km/s (or Mach 36). For spacecraft returning from Mars, the reentry velocity would be as high as 13 km/s (over Mach 40). These far exceed the reentry velocities of LEO spacecraft, and thus the heating problem is also more severe.

https://doi.org/10.1017/9781009030991.002 Published online by Cambridge University Press

Hypersonic flight also occurs when a spacecraft enters into the atmosphere of another planet or moon that has an atmosphere of its own. The entry velocity into Mars' atmosphere is typically around 6 km/s. The entry velocity into Jupiter's atmosphere is much higher. While the entry velocity at Mars is no higher than that for Earth reentry from LEO, the Martian atmosphere presents other challenges. Because of the very low atmospheric pressure and density in the Martian atmosphere, it is difficult to use aerodynamic drag to rapidly decelerate and land the entry spacecraft safely. This is especially an issue for landing much heavier manned spacecraft in future missions.

Another occurrence of hypersonic flight is when an aircraft cruises in the atmosphere at a hypersonic speed, or when a trans-atmospheric vehicle is being accelerated from subsonic speeds through the atmosphere in order to reach the orbit. For the latter, currently, access to space is accomplished using rockets. Ascending rockets encounter hypersonic conditions at relatively high altitudes near the fringe of the atmosphere. In the future, if the accelerator vehicle is propelled by air-breathing propulsion rather than by rocket, it would need to stay in a sufficiently dense part of the atmosphere to ingest adequate air for the generation of thrust, thereby lengthening the duration and intensifying the exposure to hypersonic conditions.

Before we delve into the subject of hypersonic ground testing facilities, we will first look at what kind of hypersonic flights we expect to see in the future. These provide good indications of the needs that are called for in testing them. It is only after a vehicle design has been carefully evaluated in ground facilities before flight testing can proceed. Indeed, the development of hypersonic flight vehicles is very much paced by the ability to test them on the ground.

1.1 Hypersonic Flight for the Future

1.1.1 Earth-Orbiting Spacecraft

Although still infrequent, the number of space flights is steadily increasing. Most of the flights are for access to the Earth orbits, with the majority being the launching of commercial satellites, such as those for communication, Earth observation, navigation, and air traffic tracking. Space flights are also regularly needed to ferry supplies to the International Space Station (ISS) and to transport crew members to and from it. Increasingly, scientists are exploiting space-based platforms to avoid the distortion of Earth's atmosphere by putting telescopes in the orbit. The Hubble Space Telescope is the world's first space-based optical telescope that has obtained amazing images of distant universe. The Transiting Exoplanet Survey Satellite (TESS) is another space telescope that was launched in April 2018 to search for exoplanets.

Today, besides the major space powers (United States, Russia, and Europe), more and more countries are developing the capability to construct and launch spacecraft. For example, China already launched more rockets into the orbit than any other country in 2018. Furthermore, spaceflight is no longer the sole purview of government space agencies. Private space transportation companies now develop and launch their

https://doi.org/10.1017/9781009030991.002 Published online by Cambridge University Press

own spacecraft, such as the SpaceX Dragon and Orbital-ATK (now Northrop Grumman) Cygnus, which are being used to deliver supplies to the ISS (Arney 2016).

The number of space launches will further increase as the need to place satellites into orbit continues to grow. The rise in commercial demand is particularly remarkable. Currently, most communication satellites are placed in geostationary Earth orbit (GEO). However, because of the long distance between the satellite and the ground, it takes a relatively long time (0.24 s) for the radio signals to travel to the satellite and back. The long delay results in high latency. With the rapid growth in Internet usage, there is a great desire to place communication satellites in LEOs. But because a low-orbit satellite can only serve a small local region, many such satellites are required to cover the entire globe. Since the 2010s, the private sector has invested heavily to build constellations of small satellites for communication and other applications. As examples, Amazon plans to launch a constellation of thousands of LEO internet satellites to provide low-latency, high-speed broadband network connectivity for users around the world. SpaceX's Starlink mission is already in the process of deploying its own mega-constellation of up to 12,000 LEO satellites to provide worldwide internet connections (Hofactor 2020a).

Currently, rockets have been used exclusively for launching vehicles to space. However, rockets are inefficient and expensive as they are nonreusable and the fact that they must carry the oxidizer means that there is little mass left for carrying payloads. The tremendous growth in the demand for commercial satellites is an impetus to develop alternative methods for conducting space launches. Already, private companies such as SpaceX and Blue Origin are making progress in reusable rockets (Klotz 2017). The SpaceX Falcon 9 is a partially reusable two-stage rocket launcher. After separating from the second stage, the first stage is capable of landing itself vertically on land or at sea, which will then be refurbished for reuse. Falcon 9 has already been used to launch the Dragon spacecraft to the ISS (Hadhazy 2017). Blue Origin's New Shephard rocket is also a two-stage rocket launching system capable of vertical takeoff and vertical landing so that the first stage can be reused (Klotz 2017).

Reusability together with small-size satellites allows Falcon 9 to launch 60 satellites in a single launch. However, the inherent disadvantage of needing to carry its own oxidizer still remains. To further improve launch efficiency and reduce cost, future technology will need to exploit hypersonic air-breathing propulsion.

1.1.2 Moon Exploration

In the field of science, there is also a growing interest for space exploration, and the Moon is a prime destination. Since Apollo 17 astronauts last stepped on the Moon in 1972, only robotic missions have taken place, and there have not been manned return flights. But there is a great interest in further exploring the Moon and using it as a base to explore Mars.

Besides the United States, there are already a number of countries that have executed or are planning missions to go to the Moon. India launched its first lunar probe, Chandrayaan-1, in October 2008, which started orbiting the Moon in November

https://doi.org/10.1017/9781009030991.002 Published online by Cambridge University Press

2008. The probe's Terrain Mapping Camera was used to produce a high-definition map of the Moon. The Moon Mineralogy Mapper (M^3), a NASA instrument on board the orbiter, has confirmed the magma ocean hypothesis that the Moon was once completely molten (*Economic Times* 2009). The Miniature Synthetic Aperture Radar (Mini-SAR), another NASA instrument, detected the existence of water across wide expanses of the Moon's polar regions, which was later confirmed by the M^3 infrared data (NASA 2009). A second mission, the Chandrayaan-2 orbiter and lander, was intended as a follow-up to Chandrayaan-1's discovery of water and to identify potential water sources that may support humans to set up a base on the Moon. It was launched in July 2019 and reached the Moon's orbit in August 2019. However, the landing was unsuccessful, and the lander crashed on the Moon's surface (Singh et al. 2019).

Between 2007 and 2020, China successfully landed three spacecraft on the surface of the Moon. Chang'e-3 landed on the Moon on December 14, 2013 (Barbosa 2013) and became the first spacecraft to soft-land on the Moon since NASA's last manned mission, Apollo 17, on December 19, 1972, and the former Soviet Union's unmanned spacecraft, Luna 24, on August 22, 1976. Chang'e-3 carried a lunar rover, Yutu, which was designed to conduct surface topology and geology surveys, as well as astronomical observations. Chang'e-4 was originally built as a backup for Chang'e-3 and became available after Chang'e-3 landed successfully in 2013. On January 3, 2019, Chang'e-4 achieved the milestone of the first landing on the far side of the Moon (Hadhazy 2019). The lunar far side is distinctly different from the near side. It has relatively few lunar maria, which were formed by volcanic eruptions, but has more craters. The selected landing site is within the von Karman crater in the South Pole–Aitken basin, which is itself the oldest, largest, and deepest impact crater on the Moon. The basin is of particular interest because the powerful impact that created it 3.9 billion years ago may have ejected a vast amount of deep mantle material that remain undisturbed since the impact (Hadhazy 2019). Examining the exposed material may provide insights into the formation of the Moon and the earth as well.

Another significance of the Chang'e-4 mission is the establishment of the communication link between the earth and the Moon's far side. Because the Moon's body blocks direct communication between the earth and the Moon's far side, it had impeded lunar far-side missions. To overcome this, a relay communication satellite, Queqiao, was launched ahead of the Chang'e-4 spacecraft to a halo orbit near the Earth–Moon Lagrange point L_2, about 60,000 km beyond the Moon (Hadhazy 2019). The relay satellite provides line-of-sight links with both the Moon's far side and the earth, which may serve as a key space infrastructure for the international community, thereby opening up further opportunities for the exploration of the lunar far side.

Chang'e-5 is a lunar sample return mission that was launched on November 23, 2020. Landing took place on December 1, 2020, in the Mons Rümker region of Oceanus Procellarum. Samples were collected on the lunar surface as well as by drilling up to 2 meters into the lunar regolith. Past orbital observations indicate that the area sampled has a relatively young geological age. Determination of the samples' age and composition would yield insights into late-stage geological activities on the

Moon. Following sample collection, the ascender module lifted off from the lunar surface on December 3 and rendezvoused with the orbiter on December 5. On December 16, the return capsule reentered Earth's atmosphere at a velocity of 11 km/s and landed successfully (eoPortal Chang'e-5 n.d.).

A notable recent example of lunar mission is the Israeli Beresheet that was planned to land on the Moon in 2019. The spacecraft was designed and built by SpaceIL, a private nonprofit organization. The ambitious mission sought to make history as the first ever privately funded lunar mission. The tiny Beresheet was launched atop a SpaceX Falcon 9 rocket in February 2019. The spacecraft reached the intended landing site in April 2019, but because of engine malfunction, it was crashed upon landing (Aharonson et al. 2020). Nevertheless, the mission was a partial success for completing the long journey and coming so close to landing on the Moon successfully.

Another private company, Blue Origin, has proposed a plan for commercial Moon landing using a new Moon lander Blue Moon. Blue Origin envisions the lander to serve as an early step to develop an infrastructure for lunar exploration and pave the way for the creation of space colonies on the Moon (Hofactor 2020b). Clearly, the stage is set to hasten the exploration of the Moon, with crew return flights to occur eventually. This will fuel the need for designing the reentry capsules for such missions.

1.1.3 Near-Earth Objects

Near-Earth objects (NEOs) are comets and asteroids that have orbits that bring them into Earth's neighborhood. NEOs are the primitive leftover building blocks of the solar system. They are of particular interest because their state has remained relatively unchanged since the formation of the solar system some 4.6 billion years ago. They can provide valuable information on the chemical composition of the primordial mixture from which the planets were originally formed.

There have already been a number of flyby missions to explore NEOs since 1978. NASA's Near Earth Asteroid Rendezvous Shoemaker (NEAR Shoemaker) became the first spacecraft to land on an asteroid called Eros on February 12, 2001 (McCurdy 2005). Stardust, another NASA mission, is of significance here as it was the first to return samples from a comet to Earth, and thus hypersonic reentry flight. The Stardust spacecraft encountered Comet Wild 2 on January 2, 2004. During the flyby, Stardust deployed the Sample Collection Plate to collect dust grains from the coma of the comet (Siddiqi 2018). On January 15, 2006, the Sample Return Capsule successfully separated from Stardust and reentered Earth's atmosphere at a velocity of 12.9 km/s, the fastest reentry speed into Earth's atmosphere ever achieved by a man-made object (Desai et al. 2006).

Hayabusa was a robotic spacecraft developed by the Japan Aerospace Exploration Agency (JAXA) to collect samples from the small near-Earth asteroid 25143 Itokawa and return them to Earth. The spacecraft was not intended to land on the asteroid but simply to touch the surface with its sample-capturing device and then moves away. In November 2005, Hayabusa retrieved samples from Itokawa (Grinstead et al. 2011).

The reentry capsule carrying the collected samples reentered Earth's atmosphere in June 2010. At a reentry velocity of 12.2 km/s, it became the second fastest reentry into Earth's atmosphere after NASA's Stardust reentry (Grinstead et al. 2011).

Hayabusa 2 is JAXA's second asteroid sample return mission. It was launched on December 3, 2014, and it arrived at asteroid 162173 Ryugu on June 27, 2018. On February 21, 2019, the spacecraft approached the surface of Ryugu to conduct surface sampling (eoPortal Hayabusa-2 n.d.) A 5-g tantalum projectile was fired at 300 m/s into the asteroid's surface, and the ejected particles were collected by a catcher in the spacecraft (JAXA 2019). On April 5, 2019, subsurface sampling was initiated by firing a 2-kg copper projectile at 2 km/s to excavate deeper materials that have not been subjected to space weathering. The spacecraft returned to the impact site on April 25, 2019, to confirm that a crater was created. On July 11, 2019, the spacecraft touched down on the asteroid and collected samples from inside the crater. The spacecraft started its return journey to Earth on November 13, 2019. On December 6, 2020, the sample return capsule executed reentry to Earth at a velocity of 12 km/s (eoPortal Hayabusa-2 n.d.)

The NASA OSIRIS-REx (Origins, Spectral Interpretation, Resource Identification, Security, Regolith Explorer) is an asteroid study and sample-return mission. If successful, it will be the first spacecraft from the United States to return samples from an asteroid. It was launched in September 2016 and reached the proximity of the asteroid Bennu in December 2018. Sample collection was completed in October 2020 and the reentry to Earth is expected to occur in September 2023 (NASA 2020). Besides being a primitive asteroid that has not significantly changed since its formation several billion years ago, it is also a potentially hazardous asteroid, as it has a small probability of impacting Earth in the late twenty-second century. The samples will allow the determination of the asteroid's physical and chemical properties. Another mission objective is to study the effect of nonuniform sunlight heating on the asteroid's rotating body and its impact on Bennu's orbit. The findings will be used to develop better estimates of the asteroid's impact probability with Earth (Lauretta et al. 2017).

Besides NASA and JAXA, the European Space Agency (ESA) has sent the Rosetta spacecraft to study Comet 67P/Churyumov–Gerasimenko. Its lander module, Philae, performed the first successful landing on a comet on November 12, 2014 (Costa et al. 2016). China is proposing to send a probe to collect samples from asteroid 2016 HO3 (Kamo'oalewa). The probe will fly back to the proximity of Earth, and a reentry capsule will be released to return the samples to Earth. After that, the probe will resume its journey to the main asteroid belt to explore Comet 133P (Gibney 2019).

1.1.4 Mars Exploration

There is a lot of interest to explore and study Mars, the most accessible planet in the solar system. There have already been a number of missions that flew robotic devices to orbit and land on Mars. As of February 2021, the United States had successfully deployed five rovers (Sojourner, Spirit and Opportunity, Curiosity, and Perseverance) to Mars. The latest rover was Perseverance of NASA's Mars 2020 mission. It was

https://doi.org/10.1017/9781009030991.002 Published online by Cambridge University Press

launched on July 30, 2020, and landed on Mars on February 18, 2021, in Jezero Crater, a site that was once an ancient lake. The collected rock and soil samples could potentially be returned to Earth in future missions (NASA Mars 2021, NASA Perseverance 2020). NASA's Mars 2020 mission was joined by two other Mars missions. On July 20, 2020, the United Arab Emirates Space Agency's Hope spacecraft was launched from Tanegashima Space Center, Japan, with a Japanese rocket H-IIA. It entered Mars orbit on February 9, 2021, to study the atmosphere of Mars for two years (Abbany 2021). China's Tianwien-1 was launched from the Wenchang Spacecraft Launch Site on July 23, 2020, and entered Mars orbit on February 10, 2021. The spacecraft consists of an orbiter and a lander, with the latter carrying a rover, Zhurong, that was scheduled to land in May 2021 to explore the Mars surface (Abbany 2021). On May 14, 2021, Zhurong successfully landed on Utopia Planitia – the vast Martian plain where the NASA Viking 2 spacecraft previously landed in the 1970s (Planetary Society n.d.).

The scientific goals for these missions are to determine whether Mars has ever had and has still water, and whether it has chemicals necessary for living organisms to grow. These questions cannot be answered easily using the instruments transported to Mars. Thus, there is a strong desire to return Martian samples to Earth for detailed analysis. The ultimate goal is to send humans to explore Mars and return them back safely.

Although Mars exploration has been a goal of national space programs since the 1960s, necessary technologies to accomplish manned missions are still being developed. While NASA does not yet have definite plans for a human Mars mission, SpaceX is developing the Falcon Heavy rocket and is planning to use it for crewed Mars missions (SpaceX Falcon 2021). We can expect the increase in the need for the design of vehicles for atmospheric entry into Mars and reentry to Earth from Mars exploration missions.

1.1.5 Other Planets and Moons

There are other interesting planets and moons to explore. For example, Titan, which is Saturn's largest moon and is the second-largest moon in the solar system after Jupiter's Ganymede. It is the only planetary body other than Earth in our solar system with a thick nitrogen atmosphere. It has a surface pressure about 1.5 times that on Earth. Methane is the second-most abundant atmospheric constituent on Titan, but as it is constantly destroyed by solar UV, cosmic rays, and electrons from Saturn's magnetosphere (Owen et al. 1997), it leads to the question of how it gets replenished in Titan (Lebreton et al. 2005). Are there hydrocarbon oceans that serve as reservoirs for Titan's atmospheric methane? Another significance of Titan is that its atmosphere is similar to that of early Earth when free molecular oxygen had not existed yet. The absence of molecular oxygen is known to be beneficial for the origin of life. Therefore, Titan can serve as a planet-sized laboratory of a primitive Earth atmosphere to study how life began (Owen et al. 1997).

The Huygens probe was part of the Cassini–Huygens mission to investigate Titan. It was released from the Cassini orbiter and headed toward Titan on December 25,

https://doi.org/10.1017/9781009030991.002 Published online by Cambridge University Press

2004. On January 14, 2005, the probe entered the top layers of Titan's atmosphere at an altitude of approximately 1,400 km with a speed of 6 km/s. It then decelerated rapidly to 400 m/s (approximately Mach 1.5) at an altitude of about 155 km in less than 5 min, at a point where the main parachute was deployed. The descent took about 2.5 hours before it landed successfully on Titan (Lebreton et al. 2005).

Although the Cassini–Huygens spacecraft had spent 13 years orbiting and observing Saturn, and its journey to Saturn included flybys of Venus, the asteroid 2685 Masursky, Jupiter, and Saturn's other moons (Phoebe, Enceladus, Iapetus, Rhea, Hyperion, and Dione), its entry into Titan's atmosphere was the highlight as it was the first ever landing in the outer solar system and on a moon other than that of Earth (Lebreton & Matson 2002). Huygens' data provided valuable information on the physical properties of Titan's atmosphere as well as the features of its surface. However, much more is needed to understand this moon, and the answers to the many new and remaining questions will have to wait for future exploration efforts.

Another interesting planet to explore is the gas giant Jupiter that is the largest planet in the solar system. On December 7, 1995, the Galileo probe descended into the Jovian atmosphere. At 48 km/s, the atmospheric entry into Jupiter is the most severe for any human-made spacecraft. During the descent, the probe collected data on Jupiter's atmospheric conditions and composition for 61 min until the transmitter failed due to the enormous atmospheric pressure (Siddiqi 2018). Much longer missions to study Jupiter have also been proposed. One of them uses an autonomous supersonic aircraft powered by a nuclear ramjet engine that can be transported in a spacecraft similar to the size of that which performed the Galileo mission (Maise et al. 2003, Sforza 2012). After arriving at Jupiter, an entry capsule carrying the nuclear ramjet will enter into the Jovian atmosphere. When the capsule decelerates to about Mach 3, the ramjet separates from it, and then the nuclear engine starts and uses the unlimited hydrogen in the Jovian atmosphere as a propellant to propel the vehicle that would then fly continuously and collect data for months. Hydrogen is an excellent propellant because of its low molecular weight, and so the nuclear ramjet is ideal for exploration in the two largest gas giants, Jupiter and Saturn, with both having hydrogen as their main atmospheric constituent. However, because essentially any gas could be used as a propellant, the nuclear ramjet could operate in any planetary atmosphere.

1.1.6 Suborbital Hypersonic Flight and Air-breathing Propulsion

We now turn our attention to suborbital hypersonic flight. Entries into Earth's and other celestial bodies' atmospheres are not the only conditions that involve hypersonic flight. Hypersonic flight also occurs when an aircraft travels within the atmosphere at hypersonic speeds. Although rockets are currently used to launch spacecraft to space, they only reach hypersonic speeds as they approach the upper edge of Earth's atmosphere.

A major disadvantage of rockets is that they must carry the oxidizer on the vehicle, which means that the amount of payload that can be carried is severely limited.

https://doi.org/10.1017/9781009030991.002 Published online by Cambridge University Press

To overcome this, an air-breathing propulsion system that utilizes the surrounding air, which is plentiful in the atmosphere, would free up valuable vehicle mass and space for carrying payloads. Such air-breathing propulsion systems could use a combination of turbine engine, ramjet, scramjet, and rocket to accelerate the aircraft-like vehicle gradually from the ground to hypersonic speeds. As the vehicle reaches the upper atmosphere where the air is too thin to support air-breathing propulsion, it transitions to rocket power for the final orbit insertion.

Another application of hypersonic flight is suborbital cruise. In this regard, an air-breathing engine would propel the aircraft to cruise at hypersonic speeds over a long distance. Although rockets can also cruise at high Mach numbers in an atmosphere, their range is limited because of the burden of carrying their own oxidizer.

Whether air-breathing engines are used for accelerating vehicles to space or for suborbital cruise, the hypersonic vehicles involved have some key differences from those used for atmospheric entry. For atmospheric entry, the main objective is to decelerate the vehicle as rapidly as possible from orbital or superorbital speeds down to subsonic values. The vehicle shape is, therefore, designed for high drag and for minimizing extreme aeroheating. This results in blunt-shaped bodies, especially when convective heating dominates over radiative heating.

On the other hand, hypersonic vehicles propelled by air-breathing engines would have to stay in the much denser part of the atmosphere for a much longer time, as a large amount of air is needed to be ingested to generate thrust. Thus, hypersonic atmospheric flights can also experience severe aeroheating just as for flights during atmospheric entry. Furthermore, because hypersonic cruise vehicles must also have high aerodynamic performance, that is, good lift–drag characteristics, the body shape would need to be slender rather than blunt, which allows the extreme aeroheating to have a larger impact on the vehicle.

The supersonic combustion ramjet (scramjet) has been studied since the 1960s. The first aircraft that achieved hypersonic speed was the X-15. This rocket-powered plane was developed to study hypersonic flight and was to be used as a test bed to test hypersonic air-breathing engines. The X-15 reached a speed of Mach 6.7 in 1967, but the program was canceled in 1968 (Urzay 2018). The most ambitious hypersonic program that involves air-breathing propulsion was the National Aero-Space Plane (NASP) in the United States to create a scramjet-powered single-stage-to-orbit space plane. The program started in the late 1980s but was canceled in 1993 with no test flight flown (Urzay 2018). A milestone was achieved in 2004 when NASA successfully flew a self-propelled scramjet-powered unmanned vehicle, X-43A, at Mach 10 (Urzay 2018). As the scramjet operated only for about 10 s during the test flight, the X-43A does not represent a true aerospace plane that can cruise long distances through the atmosphere. The next major program in the United States to progress scramjet-powered flight was the X-51, which was started in 2004. One of the program's goals was to extend the operation of scramjet–powered flight from 10 s to several minutes. In May 2013, an unmanned X-51A successfully flew at Mach 5.1. The scramjet engine burned for 210 s to accelerate the vehicle to Mach 5.1, in the longest ever mission for a vehicle of its kind (Urzay 2018).

Another type of hypersonic cruise is that of the hypersonic glide vehicle (HGV). It is a class of suborbital flight vehicle that is boosted by a rocket to the high upper atmosphere, which then employs aerodynamic lift to glide over a long range at high altitudes before reentering the atmosphere. The DARPA Falcon (Defense Advanced Research Projects Agency's Force Application and Launch from CONtinental United States) program test flew two Hypersonic Technology Vehicle 2 (HTV-2): one in 2010 and another in 2011. The HTV-2 is an experimental HGV capable of flying at Mach 20 near the edge of the atmosphere (Malik 2012). As gliders, the HTV-2s did not have propulsion. However, technologies being tested have great relevance to scramjet-propelled hypersonic flight. In contrast to other reentry vehicles, the HTV-2 has a slender shape to improve its aerodynamic performance in order to achieve the flight range. Both this and the long flight duration pose a major challenge regarding aeroheating. Since 2014, China has tested various hypersonic gliders, such as the DF-ZF, reaching speeds between Mach 5 and Mach 10 (Wood & Cliff 2020). Russia also tested the Avangard HGV from 2015 to 2018, which is designed to operate at Mach 20 at the edge of the atmosphere (Button 2018).

Up until the 2000s, the development of hypersonic atmospheric flight had not been sustainable, and developmental efforts were followed by periods of stagnation. However, research and development seems to have intensified again in the 2010s. The scramjet is a high risk, but potentially a high pay-off, technology. The countries that can first master this technology and exploiting it in weapons systems will have a significant advantage over the others. Thus, it is not surprising to find that countries are racing to progress the readiness of hypersonic air-breathing propulsion.

In the United States, Lockheed-Martin is reportedly developing a hypersonic SR-72 vehicle capable of reaching Mach 6 as a successor of the retired reconnaissance plane SR-71 (Norris 2013). Reaction Engines in the United Kingdom is testing the Synergetic Air Breathing Rocket Engine (SABRE) hybrid air-breathing rocket engine that would rapidly precool the incoming air with liquid hydrogen to allow a gas turbine engine to continue working up to Mach 5.5, at which point, the engine would transition to rocket mode and accelerate the aircraft to orbit (Odom & Johnston 2018). The Indian Space Research Organization (ISRO) conducted an experimental hydrogen-fueled Mach 6 scramjet engine that operated for about 5 s in 2018 (Odom & Johnston 2018). In Japan, JAXA plans to test an experimental airplane, HIMICO (High-Mach Integrated Control Experiment), which uses liquid hydrogen to precool the incoming air in order to extend the operability of conventional turbine engines to Mach 5 (Odom & Johnston 2018). Brazil plans to flight test a prototype of the 41-X unmanned hypersonic airplane with a scramjet engine at an altitude of 30 km and a Mach number of 7 (Martos et al. 2017).

Intense research is currently being undertaken in various countries to develop the scramjet into a mature technology. The initial application of hypersonic air-breathing propulsion will always be in weapons of destruction, but eventually, the peaceful application of it in the next generation transport would hopefully follow to benefit all mankind.

1.2 Hypersonic Aerothermodynamics: Key Issues and Research Progress

A selected list of key issues related to hypersonic flow and the development of hypersonic flow theory will be briefly discussed in this section. The list is not intended to be exhaustive, and the introductory remarks in Sections 1.2.1 to 1.2.5 below serve mainly to bring out the significance and challenges of the hypersonic flow regime rather than to explore the theory in-depth. Examples of experimental studies that have been carried out in test facilities on some of the topics will be discussed in subsequent chapters in the book.

1.2.1 Hypersonic Flow Defined

A flow is termed hypersonic when the freestream velocity U_∞ is much larger than the speed of sound a_∞. Using the definition of Mach number, which is the ratio of the velocity to the sound speed in the freestream, we have

$$M_\infty = \frac{U_\infty}{a_\infty} \gg 1. \tag{1.1}$$

The Mach number is a measure of the square root of the kinetic energy of the gas to its thermal energy. For hypersonic flows, the freestream kinetic energy is much larger than the thermal energy of the freestream fluid particles. In particular, the term "hypersonic" is used to distinguish those flows in which the velocity is so large that the conditions behind the shock waves on a body are such that the gas is no longer inert. As the freestream Mach number increases beyond 1.0, shock waves form over the body. The rise in temperature behind the shock waves, which increases with the freestream Mach number, eventually causes the gas molecules to be vibrationally excited. As the Mach number increases further, the chemical bonds that bind the molecules together start to break, leading to dissociative reactions. At even higher Mach numbers, ionization occurs. These processes are often collectively referred to as "real-gas effects."

Although it is commonly accepted that "hypersonic" refers to speeds greater than about Mach 5, there are better quantitative measures to distinguish it from the supersonic regime. Indeed, it is rather imprecise to define the threshold of "hypersonic" based on a Mach number, because the phenomena that characterize hypersonic flight depend on the flow conditions as well as on the body shape and its orientation.

In order to better define the hypersonic regime, we will examine two of its characteristics. The first is the hypersonic Mach number independence principle. The principle of hypersonic Mach number independence was first derived by Oswatitsch (1951, 1980) for a calorically perfect gas with no viscosity. The derivation of the principle can be readily found in the literature, such as the book by Anderson (2006). It can be shown that at very large freestream Mach numbers, certain nondimensional aerodynamic quantities, such as pressure coefficient, lift and wave-drag coefficients, and flow field structure become independent of the Mach number. A key parameter that characterizes Mach number independence is

https://doi.org/10.1017/9781009030991.002 Published online by Cambridge University Press

$$M_\infty^2 \sin\beta \gg 1, \tag{1.2}$$

where β is the local shock-wave angle. Equation (1.2) shows that hypersonic Mach number independence begins earlier for blunt bodies than for slender ones. For blunt bodies, sin β is large, so that Eq. (1.2) is satisfied at lower M_∞ than for slender bodies. The parameter also depends on the orientation of the flight body. For a slender body at a high angle of attack, sin β is large enough so that it fulfills the Mach number independence principle at a lower Mach number than at zero angle of attack.

While Oswatitsch's principle does not include viscous and high-temperature reacting gas effects, ballistic range measurements have demonstrated that the drag coefficients for the sphere and cone–cylinder configurations do approach their respective constant values at high Mach numbers (Charters & Thomas 1945, Stevens 1950, Hodges 1957, Cox & Crabtree 1965).

Another important feature of hypersonic flow is the occurrence of real-gas effects. At high Mach numbers, the temperature downstream of the bow shock is sufficient to cause vibrational excitation, dissociation, and even ionization. Since the post-shock temperature for a normal shock is higher than that for oblique ones, and as blunt bodies have a larger portion of the surfaces exposed to the normal shock, they experience reacting gas effects at lower Mach numbers than slender bodies. For air at a pressure of one standard atmosphere, molecular oxygen begins to dissociate at about 2,500 K. At 4,000 K, molecular oxygen is mostly dissociated, and molecular nitrogen begins to dissociate. At about 9,000 K, molecular nitrogen is mostly dissociated and ionization begins (Anderson 2006). Thus, at standard sea level freestream conditions, reacting gas effects would start at a temperature of approximately 2,500 K, which would correspond to a post-shock temperature for the freestream Mach number of about 8. However, dissociative reactions also depend on the pressure and therefore on the flight altitude. At lower pressures or high altitudes, dissociation occurs at lower temperatures and therefore lower Mach numbers.

A more illustrative picture of the level of real-gas effects experienced during flight can be obtained by relating it to the flight speed. Consider a flight body flying in Earth's atmosphere at a certain Mach number that is larger than 1, giving rise to a bow shock in front of the body. As the flight Mach number increases, the temperature of the shock-heated air will eventually be sufficiently high to cause chemical reactions to occur. The chemical composition of the air behind the normal portion of the shock can be calculated readily using a chemical equilibrium analysis (see, e.g., McBride & Gordon 1996). Shown in Figure 1.1 are the species mole fractions of the air behind a normal shock at freestream Mach numbers ranging from 1.5 to 40. For simplicity, a flight altitude of 30 km is assumed, corresponding to an ambient pressure of 1,200 Pa, temperature of 226 K, and sound speed of 302 m/s. At Mach numbers below 5, the air is quite inert, comprising N_2 and O_2 with mole fractions of 79% and 21%, respectively. At about Mach 6, dissociation of the N_2 and O_2 molecules starts and a small amount of NO is formed. At about Mach 8, a significant dissociation of O_2 to O begins and is completed near Mach 15, at which point a significant dissociation of N_2 to N

https://doi.org/10.1017/9781009030991.002 Published online by Cambridge University Press

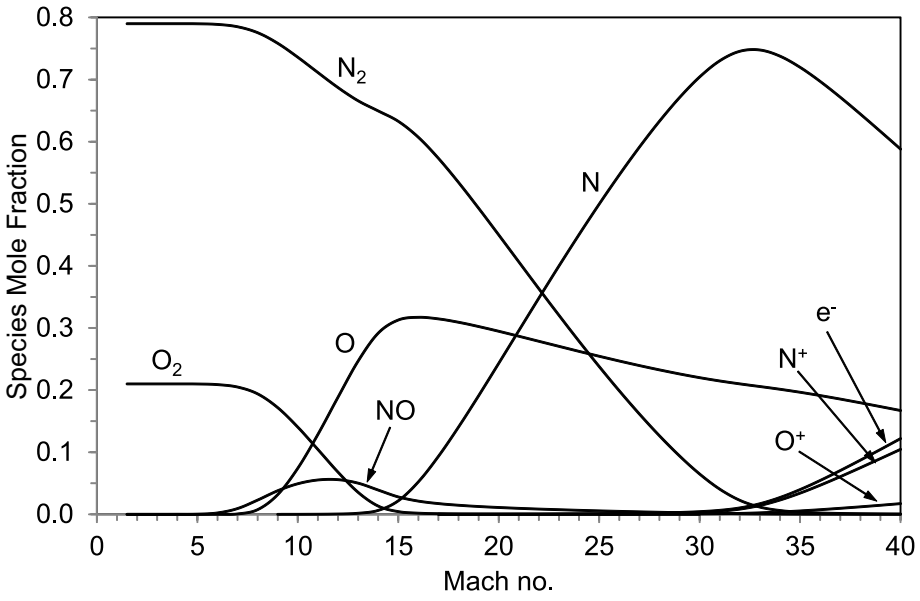

Figure 1.1 Species mole fraction of air behind a normal shock at different freestream Mach numbers at an altitude of 30 km.

starts. By about Mach 30, N_2 is completely dissociated and ionization begins, giving rise to free electrons e^- and ions N^+ and O^+. It is of interest to note three flight Mach numbers – 25, 36, and 40. Mach 25, or a flight velocity of about 7.5 km/s, is the typical reentry velocity from LEOs. As can be seen from Figure 1.1, there is a complete dissociation of O_2 and a significant dissociation of N_2 at this speed. Mach 36, or approximately 11 km/s, is encountered during a flight's reentry into the Earth's atmosphere following lunar missions. At this Mach number, N_2 is completely dissociated, and ionization has started. For spacecraft returning from missions to comets and asteroids, the Earth reentry Mach number is around 40 or a velocity of 12 km/s, at which point ionization becomes appreciable.

Since Figure 1.1 is obtained for a fixed flight altitude, and thus the freestream pressure, one should bear in mind that real-gas effects generally increase at lower pressures. A flight velocity–altitude map with regions of vibrational excitation, dissociation, and ionization superimposed over the map has been computed by Tauber et al. (1987). It provides the same information as Figure 1.1 but adds details regarding variations with the flight altitude. Note also that the intensity of real-gas effects depends on the vehicle's shape and orientation as well. For shock-wave angles smaller than that for a normal shock, as encountered on slender bodies, the post-shock temperature will be lower, leading to weaker real-gas effects. Nevertheless, the general conclusion is that a true quantitative description of the flow encountered in hypervelocity flight must include real-gas effects.

https://doi.org/10.1017/9781009030991.002 Published online by Cambridge University Press

Note that "cold hypersonic" flows can be generated by cooling the fluid at a medium to very low temperature to decrease its sound speed so that high Mach numbers can be reached with relatively low velocities. However, such high Mach number flows must be differentiated from those in real flight because the low temperature in cold hypersonic flows precludes chemical reactions and the associated real-gas effects.

Other commonly used terms to describe extremely high-velocity conditions are "hypervelocity" and "high enthalpy," both avoid the ambiguity of low-temperature hypersonic flows. "Hypervelocity" represents both high Mach number and high velocity. "High enthalpy," or more appropriately high total enthalpy, essentially means high velocity. This can be seen in the definition of total or stagnation enthalpy, which is the sum of static enthalpy and kinetic energy:

$$h_t = h + \frac{U_\infty^2}{2}. \tag{1.3}$$

At extremely high velocities, the total enthalpy h_t is dominated by the kinetic energy of the flow. Both "hypervelocity" and "high enthalpy" are commonly used in the literature in the context of atmospheric entry events, and thus they are more precise terms when characterizing flows with significant real-gas effects.

The preceding discussions on Mach number independence and reacting gas effects indicate that the Mach number is no longer the best parameter to characterize hypersonic flows. At large Mach numbers, the kinetic energy far exceeds the thermal energy. A more suitable reference energy quantity, which reflects that the substantial reacting processes are taking place, can be utilized to construct a different nondimensional parameter. For example, for reentry from LEOs, the dissociation energy of nitrogen could be used as a reference quantity. However, this is not a widely accepted practice.

1.2.2 Stagnation Region

Consider a flight vehicle flying at a very high velocity. When viewed in the reference frame of the vehicle, as the incoming air is decelerated and brought to rest near the vehicle's surface, the flow kinetic energy is converted into thermal energy, thus heating both the airflow and the vehicle body. The shock wave formed around the body heats the airflow, while the intense friction in the boundary layer heats the body.

Temperatures and surface pressures are usually the greatest at the stagnation point, which is downstream of the normal portion of the bow shock wave over the vehicle. This leads to extremely high heat transfer to the vehicle.

The heat transfer in the stagnation region became an important problem early on in the development of hypersonic flow theory. In the 1950s, aerodynamic heating was a major challenge for the development of intercontinental ballistic missiles (ICBMs) as ICBMs have to endure extreme heating during reentry into the atmosphere. It was initially thought that a reentry body should have a conical sharp nose with a pointed tip, much like an artillery shell. However, with the sharp-nose cone, a conical shock wave is attached that is relatively weak and that does little to heat the airflow, whereas the severe heat transfer from the boundary layer into the vehicle's body could melt the sharp nose and even destroy the vehicle structure.

https://doi.org/10.1017/9781009030991.002 Published online by Cambridge University Press

Harvey Allen came up with a revolutionary idea that by diverting more of the reentry energy into the airflow, there is less left to heat the vehicle. This is achieved by using a blunt nose that generates a strong detached shock wave standing ahead of the vehicle, so that most of the heat goes off the surface and into the flowfield, not into the vehicle.

Allen's blunt-body analysis (Allen & Eggers 1953) used simplified assumptions that neglected chemical reactions and radiation to show that the maximum convective heat transfer rate q_{conv} is inversely proportional to the square root of the leading-edge nose radius at the stagnation point:

$$q_{\text{conv}} \propto \frac{1}{\sqrt{R_N}}. \tag{1.4}$$

Thus, to reduce the stagnation-point heat transfer rate, the nose radius R_N should be as large as possible. The blunt-body concept led to the choice of the manned reentry capsule shapes for the Mercury, Gemini, and Apollo vehicles. Indeed, all successful reentry bodies have been blunt because of this concept. Allen's original report (Allen & Eggers 1953) was classified as it was intended for ballistic missile applications, and it became declassified and publicly released in 1958 (Allen & Eggers 1958).

The chemically reactive nature of hypersonic flows can have a profound influence on the heating of the vehicle's surface. Fay and Riddell (1958) formulated the equations to calculate the convective heat transfer rate at the stagnation point of a blunt body in chemically reacting air. Fay and Riddell's theory was derived using laminar boundary-layer equations applied to the stagnation region of spherical and cylindrical geometries. The equations include different possible scenarios: chemical equilibrium and frozen boundary layers, and catalytic and non-catalytic walls.

The stagnation-point heat transfer obtained from Fay and Riddell's equations could be used both to verify the validity of wind-tunnel measurements and also computational fluid dynamics (CFD) solutions. It is also often used as a denominator to construct a nondimensional heat transfer ratio at different locations along the vehicle's surface. This dimensionless parameter could then be used to extrapolate wind-tunnel model measurements to actual flight conditions.

Fay and Riddell (1958) noted that while the process of dissociation and recombination is important for determining the thermodynamic state of the air throughout the flowfield, the effect on heat transfer is secondary. Also, the result is dominated by the freestream flow properties, with only weak dependence on the condition of the wall's surface. Thus, an approximate value for the stagnation-point convective heat transfer rate for a sphere can be computed using the following simple equation (Bertin 1994):

$$q_{\text{conv}} = \frac{C}{\sqrt{R_N}} \rho_\infty^{0.5} U_\infty^3, \tag{1.5}$$

where ρ_∞ and U_∞ are the freestream density and velocity, respectively, R_N is the nose radius, and C is a constant. For reentry conditions into Earth, Tauber (1989) obtained an identical approximate equation where C equals 1.83×10^{-4} when SI units are used and the resulting heat transfer rate is in W/m^2. Similar correlations have been obtained by other authors with slightly different values of the exponents for the density and

https://doi.org/10.1017/9781009030991.002 Published online by Cambridge University Press

velocity. Equivalent equations for different atmospheric gases in other planets have also been obtained by various authors, such as Marvin and Deiwert (1965), Sutton and Graves (1971), and Justus and Braun (2007).

The significance of Eq. (1.5) is that the convective heat transfer rate at the stagnation point scales inversely with the square root of the nose radius, as originally pointed out by Allen and Eggers (1953). The larger the nose radius, the smaller the stagnation-point heat transfer rate. To minimize convective heating, blunt forebody shapes with large nose radii have been used on reentry vehicles.

For many problems of interest, such as those for suborbital flight and the reentry from LEOs, the heat transfer is dominated by convective heating. However, when the flight speed reaches about 10 km/s, radiative heating becomes significant and will eventually exceed convective heating as flight speed increases further. For example, radiation was the dominant mode of heat transfer for the Galileo probe that entered Jupiter's atmosphere at a velocity of about 50 km/s.

For an emitting and nonabsorbing gas (transparent gas), the stagnation-point heat transfer rate due to radiation can be approximated by (Anderson 2006)

$$q_{\text{rad}} = \frac{E}{2} R_N \frac{\rho_\infty}{\rho_s}, \tag{1.6}$$

where E is the total energy emitted by the gas in all directions per second per unit volume, ρ_∞ and ρ_s are, respectively, the density in the freestream and behind the normal shock, and R_N is the nose radius. Equation (1.6) shows that the radiative heat transfer is directly proportional to the nose radius, whereas in Equation (1.5), the convective heat transfer is inversely proportional to the square root of the nose radius. Thus, the design of superorbital reentry vehicles would need to find a compromise between the two phenomena. To minimize convective heating, the nose radius should be made large, while to minimize radiative heating, the nose radius should be small.

With the advent of modern computers and the advances of CFD, a detailed solution of the stagnation region flowfield can be readily obtained. To achieve high-fidelity solutions, it is necessary to have accurate modeling of the physical and chemical processes at the temperatures encountered during hypersonic flight. The validation of these models requires experimental data. However, it remains extremely difficult to replicate the flow conditions in ground testing facilities.

1.2.3 Viscous Interactions

Localized high heating can also occur because of viscous effects. There are two important viscous interactions in hypersonic flow. The first is associated with the interaction between the boundary layer and the inviscid flowfield. In classical low-speed boundary-layer theory, the boundary-layer thickness is assumed to be small so that viscous effects are confined to the thin layer near the surface. The outer inviscid flow remains unaffected by the presence of the boundary layer. In the hypersonic regime, the flow deceleration from the freestream to the boundary layer converts a large amount of the freestream kinetic energy into thermal energy. If the static

https://doi.org/10.1017/9781009030991.002 Published online by Cambridge University Press

pressure remains uniform across the boundary layer, the density becomes very low in the boundary layer, thus making it exceptionally thick. The presence of the boundary layer can weakly or strongly affect the inviscid outer flow, which in turn feeds back to alter the characteristics of the boundary layer. Such interaction between the outer and viscous flows is referred to as pressure interaction.

The second interaction is the shock-wave/boundary-layer interaction that is due to the impingement of a strong shock wave on a boundary layer. Because of such interaction, the boundary layer is disturbed and may even separate depending on its thickness and the strength of the shock.

Shock-on-shock interaction is part of the shock-wave/boundary-layer interaction family, and it can cause high localized heating. Early studies have reported a large increase in the local heat transfer rate as an extraneous shock impinges on the leading edge of a blunt body over a wide range of Mach numbers, from 2.65 to 19 (Newlander 1961, Siler & Deskins 1964, Francis 1965, Ray & Palko 1965, Hiers & Loubsky 1967). Edney carried out a thorough investigation of shock–shock interactions and presented the definitive treatise on the entire spectrum of interaction patterns. The details of his work were documented in the Flygtekniska Försöksanstalten (FFA) report (Edney 1968a), and a summary was published in Edney (1968b).

Shock–shock interaction's potential to cause catastrophic failure was fully realized in 1967 when a rocket-powered X-15 aircraft that carried a dummy ramjet engine suffered severe damage to the engine support pylon during a Mach 6.7 flight. The shock wave that propagated from the nose cone of the dummy engine impinged on the pylon, causing the interaction between the conical shock with the bow shock around the pylon. This interaction generated intense heat that burned through the pylon resulting in the loss of the dummy engine; it also caused severe damage to the aircraft's internal structure (Watts 1968).

Shock–shock interaction is of great importance in hypersonic flight as it can cause severe heating that can result in major structural damages, as shown in the case of the X-15 flight above. The interaction has great implications for hypersonic air-breathing engines as the leading-edge shock wave originating from the vehicle forebody is often designed to impinge on the inlet cowl lip. The interaction is also a concern on winged reentry vehicles, such as the space shuttle, as the bow shock originating from the nose can impinge on the wing leading edge. Another possible occurrence is during the flight of a hypersonic missile, the bow shock that originates from the nose cone can interact with the shocks around a booster or fuel tank attached to the missile. The effects of shock–shock interaction must therefore be quantified in ground experiments in order to validate hypersonic vehicle designs.

1.2.4 Hypersonic Trim Anomaly

The high-temperature chemically reacting nature of hypersonic flow can have a large impact on aerodynamic forces and moments. This fact was not fully recognized until the Space Shuttle's first flight (STS-1). During its first reentry, the Space Shuttle Columbia experienced a much larger nose-up pitching moment than the

https://doi.org/10.1017/9781009030991.002 Published online by Cambridge University Press

preflight prediction. The body flap had to be deflected more than twice the predicted amount (15° instead of 7.5°) – almost running out of available deflection – in order to achieve trimmed flight. This phenomenon has been referred to as hypersonic trim anomaly, which was also observed in Apollo flights (Crowder & Moot 1965, Park 1996a).

The predicted aerodynamic characteristics of the Space Shuttle were based on extensive wind-tunnel testing that spanned a wide range of Mach numbers ranging from subsonic to hypersonic, as documented in the preflight Aerodynamic Design Data Book (Anon. 1980). However, although real-gas effects were considered prior to flight, the wind-tunnel data did not include conditions that could simulate high-temperature hypersonic phenomena. Thus, real-gas effects were not adequately accounted for in the preflight predictions.

Investigations were conducted to resolve the observed aerodynamic anomaly. It was found that high-temperature real-gas effects can result in the pitching moment discrepancy (Maus et al. 1984), although other mechanisms, such as viscous–rarefaction effects (Koppenwallner 1987), could also be plausible explanations (see the discussion on pages 141–147 in Bertin [1994]). Nevertheless, there has been an increasing body of literature that supports real-gas effects as the most likely cause of the pitch-up anomaly (Brauckmann et al. 1995, Park 1995, Bertin & Cummings 2006). This realization is one of the driving forces for the development of large-scale shock-tunnel facilities in the world to replicate high-temperature real-gas effects at hypersonic flight conditions. The biggest facilities, including both the HEG in Germany and HIEST in Japan, were intended to assess high-temperature real-gas effects on aerodynamic characteristics.

1.2.5 Boundary-Layer Transition

Laminar–turbulent boundary-layer transition has great importance in hypersonic flight. For reentry vehicles, boundary-layer transition can drastically increase aeroheating, further aggregating the already severe problem. For vehicles powered by air-breathing propulsion systems, much of the hypersonic flight in the atmosphere takes place at conditions where the flow is transitional. This impacts not only the external aerodynamics and heating but also the flow characteristics in the engine and thus have ramifications for its performance. In the hypersonic regime, real-gas effects can influence the state of the boundary layer, as dissociation reactions can absorb the flow energy and have a stabilizing effect.

The prediction of boundary-layer transition is always a challenge, even for low speed, incompressible flows. The problem becomes more difficult at hypervelocity conditions. One of the difficulties in developing effective prediction tools is the lack of flight and ground testing data.

Flight experiments provide the most valuable data as they are taken at the actual flow conditions (see the survey by Schneider [1999]), but these are very expensive. Thus, only a handful of hypersonic flight experiments have been conducted. Two examples of such experiments are the Reentry-F in 1968, which was a slender cone

boosted to Mach 20 (Wright & Zoby 1977) and has become a benchmark for ground experiments, and the Space Shuttle BLT experiment in 2006, which measured the effects of protuberances on the onset of transition (Berry et al. 2011). The most recent flight experiment that was specifically designed to study hypersonic boundary-layer transition was the NASA Hypersonic Boundary Layer Transition (HyBoLT) in 2008 (Chen & Berry 2010). The test model was mounted on top of an ATK rocket that was intended to collect data at Mach 5 and 7. The model is a double-sided symmetric wedge with a smooth flat plate on one side to study natural transition and a surface with roughness on the other side to study roughness transition. The flight took place on August 22, 2008, but was terminated prematurely as the rocket booster deviated off-course after lift-off (Berry et al. 2011).

On the ground, it remains a challenge to replicate the extreme flow conditions while avoiding large facility noise that can cause interference in the transition process. As will be seen in Chapter 4, significant progress has been made in using high enthalpy shock tunnels to study transition.

1.3 Simulation Requirements for Hypersonic Flow

In order to simulate high-temperature real-gas effects in ground testing facilities, a number of dimensionless parameters need to be replicated. As in other wind-tunnel simulations, the usual nondimensional parameters that need to be matched include Mach number, Reynolds number, ratio of specific heats, Prandtl number, and Lewis number. These parameters remain adequate for "cold" hypersonics where real-gas effects and chemical reactions do not dominate. Because of the high temperature and chemically reacting nature of hypersonic conditions, proper simulation requires additional parameters to be considered.

Since chemical reactions are highly sensitive to the gas composition, temperature, and pressure, it is hopeless to satisfy similarity unless the gas medium used in ground testing is the same as that in actual flight. As chemical reactions are driven by the energy content in the flow, duplication of the total enthalpy, and hence the velocity, is required. Furthermore, in order to simulate the thermochemical state of the flow over the vehicle, the duplication of Damköhler's first number, Da_1, is also required. Damköhler's first number is defined as the ratio of characteristic flow time to the chemical reaction time:

$$Da_1 = \frac{\text{Characteristic flow time}}{\text{Chemical reaction time}}. \tag{1.7}$$

Damköhler's first number is often rewritten in terms of length, as the freestream velocity can be used to construct both length scales:

$$Da_1 = \frac{\text{Characteristic flow length}}{\text{Chemical reaction length}}. \tag{1.8}$$

Thus, when Da_1 is duplicated, the same chemical reactive states occur at the same locations on a small-sized wind-tunnel model as those on the flight vehicle.

https://doi.org/10.1017/9781009030991.002 Published online by Cambridge University Press

For chemical reactions dominated by two-body molecular collisions (e.g., dissociative reactions), Damköhler's first number leads to an important scaling parameter, the binary scale, which is the product of the flow density ρ and the characteristic length L:

$$\text{Binary scale} = \rho \times L. \tag{1.9}$$

The binary scale parameter can be derived for two-body chemical reactions and can be found in Anderson (2006).

If the temperature is also duplicated – as chemical reactions are very sensitive to temperature – the static pressure scales with the density according to the perfect gas equation:

$$p = \rho RT \sim \rho. \tag{1.10}$$

Thus, binary scaling can also be stated as

$$\text{Binary scale} = p \times L. \tag{1.11}$$

Furthermore, when the velocity and temperature are also duplicated, duplicating ρL implies that the Reynolds number, Re, is automatically duplicated:

$$Re = \frac{\rho UL}{\mu}, \quad \mu = \mu(T) \text{duplicated},$$
$$Re \sim \rho L \tag{1.12}$$

The duplication of the binary scale parameter implies that to test a small-scale model in the wind tunnel, the density (and therefore the pressure) needs to be raised. Since the test flow (freestream) pressure p_∞ scales with the reservoir pressure p_0, the facility total pressure needs to be increased accordingly.

1.3.1 Atmospheric Entry

For hypervelocity blunt-body flows in which Mach number independence applies, the significance of the Mach number is overtaken by other considerations. As pointed out in Section 1.2.1, instead of the ratio of kinetic energy to the thermal energy of the gas (i.e., Mach number), the ratio of the kinetic energy to a more characteristic energy is better suited to describe the flow. For reentry into Earth's atmosphere, the dominant energy is the dissociation energy of nitrogen, which has a value of approximately 34 MJ/kg. Therefore, the total enthalpy, which is essentially the kinetic energy, or the ratio of total enthalpy to nitrogen dissociation energy can be used as a measure of a wind tunnel's capability of generating such a condition. When the atmospheric gas composition is different (such as CO_2 for Mars entry, which has a dissociation energy of approximately 12.2 MJ/kg), the characteristic dissociation energy would be different as well.

As the test flow Mach number need not match that at flight, the test flow can be expanded to a Mach number that is lower than the flight value to achieve the required freestream pressure or density to achieve binary scaling. The advantage of this is that

https://doi.org/10.1017/9781009030991.002 Published online by Cambridge University Press

by expanding to a lower Mach number, the required total pressure decreases drastically, thereby reducing the facility pressure requirements.

On the other hand, the resulting lower test flow Mach number means that the test flow temperature is higher than that in flight, thus upsetting the matching of the freestream Reynolds number and other parameters. Fortunately, at the extreme high enthalpies encountered in atmospheric entry conditions, the thermal energy downstream of the bow shock wave is very closely approximated by the freestream kinetic energy:

$$h_t \approx \frac{U_\infty^2}{2} \approx c_{p_{\text{stag}}} T_{\text{stag}}, \tag{1.13}$$

where c_p is the specific heat at constant pressure and the subscript "stag" denotes the stagnation condition. Thus, the resulting temperature on the model, particularly in the shock-heated gas in the stagnation region, is still correct.

In summary, to simulate hypervelocity atmospheric entry, the primary matching parameters are the total enthalpy and the binary scale, as the same gas composition as in real flight is used. Total enthalpy is related to the energy, or power, that can be delivered by the facility, while binary scaling is related to the pressure level that can be achieved in the facility. The extremely large total enthalpies demanded in hypervelocity testing pose the biggest difficulty to overcome, although the fulfillment of adequate pressure is also a challenge in the design of such test facilities.

1.3.2 Air-breathing Propulsion

Ground testing of air-breathing engines requires a different set of simulation parameters than those for external flows over blunt bodies. First of all, the total enthalpy (i.e., velocity) must still be duplicated. But since the body shape for vehicles that utilize air-breathing engines for propulsion is not blunt, Mach number independence does not apply. Indeed, the simulation of the forebody and engine inlet shock system requires replicating the Mach number.

Proper simulation of the combusting flow in hypersonic air-breathing engines requires matching of the first and second Damköhler numbers. The timescale of the ignition process, which is a two-body chemical reaction, is usually used in the first Damköhler number, which then results in the binary scaling parameter. However, the subsequent heat release and equilibration in the combustion process are more complex and require different scaling laws. The second Damköhler number, Da_2, is defined as the ratio of the heat release by chemical reactions to the total enthalpy (Anderson et al. 1990):

$$Da_2 = \frac{\text{Heat release by chemical reactions}}{\text{Total enthalpy}}. \tag{1.14}$$

This number is relevant to propulsion as it pertains to the heat release in burning the fuel in the engine. It may be thought of as similar to the reciprocal of the ratio of total enthalpy to dissociation energy for atmospheric entry simulations.

In addition, the engine thrust (F) is proportional to the mass flow rate ($\dot{m}_{\text{air}}$) entering the engine, as seen in the thrust equation for an air-breathing engine:

https://doi.org/10.1017/9781009030991.002 Published online by Cambridge University Press

$$F = \dot{m}_{\text{air}}\left(U_{\text{exhaust}} - U_{\infty}\right) = \rho_{\infty} U_{\infty} A_{\text{capture}}\left(U_{\text{exhaust}} - U_{\infty}\right), \tag{1.15}$$

where U_{exhaust} and U_{∞} are the velocities at the exhaust and in the freestream, and A_{capture} is the inlet capture area. As the engine is scaled down in ground testing, the mass flow rate per unit area $(\rho_{\infty} U_{\infty})$ must be replicated to correctly simulate the thrust produced.

Note, however, that the requirements of replicating the binary scaling $(\rho_{\infty} L)$ and mass per unit area $(\rho_{\infty} U_{\infty})$ are incompatible with each other. For a small engine model of length L, binary scaling means ρ_{∞} must increase. But if ρ_{∞} is increased, the mass flow per unit area cannot be matched. This means that the test engine would generate a higher thrust for its size than the flight engine. To avoid this problem, ground testing of air-breathing engines should be carried out at, or close to, the same scale as the flight vehicle.

In many practical combustors, the timescale of the combustion process is dominated by mixing rather than by chemical reactions. In this so-called mixing-controlled combustion, although chemical reactions still take finite time, the process of fuel–air mixing requires far longer time and becomes the dominating timescale. Thus, the duplication of the binary scale parameter is not required. Furthermore, if the combustor flow is fully turbulent, which is an idealization, the boundary-layer thickness δ and mixing effects scale with the one-fifth power of the Reynolds number:

$$\frac{\delta}{L} \sim \frac{1}{Re^{1/5}}, \quad Re = \frac{\rho_{\infty} U_{\infty} L}{\mu_{\infty}}, \tag{1.16}$$

so that the mixing layer scales with the four-fifths power of the length:

$$\delta \sim \frac{L}{L^{1/5}} = L^{4/5}. \tag{1.17}$$

Fuel–air mixing then scales approximately linearly with the model size. This helps greatly the ground simulation of hypersonic air-breathing propulsion when the above ideal conditions are met.

Note also that the matching of $\rho_{\infty} U_{\infty}$ implies that the freestream dynamic pressure $\left(\frac{1}{2}\rho_{\infty} U_{\infty}^2\right)$ is automatically duplicated. Furthermore, as the dynamic pressure q_{∞} can be rewritten in terms of the static pressure q_{∞} and the Mach number M_{∞}:

$$q_{\infty} = \frac{1}{2}\rho_{\infty} U_{\infty}^2 = \frac{1}{2}\gamma_{\infty} p_{\infty} M_{\infty}^2, \tag{1.18}$$

duplicating the dynamic pressure and the Mach number implies that the static pressure is also duplicated. This is also equivalent to the duplication of the flight total pressure.

The significance of the last point is that hypersonic air-breathing engines encounter extremely high flight total pressures. For example, at a flight Mach number of 15, the freestream total pressure is of the order of 10,000 atmospheres. This represents a major challenge to ground-test hypersonic air-breathing propulsion as such pressures would exceed the structural load limits of facility components (~3,000 atmospheres).

https://doi.org/10.1017/9781009030991.002 Published online by Cambridge University Press

1.4 Hypersonic Ground Testing Facilities

1.4.1 Pulse Facilities

For ground testing of hypersonic vehicles, the necessity to duplicate the extremely high enthalpy or velocity poses a severe power requirement. Consider the testing of a reentry vehicle at an LEO reentry velocity of 7 km/s and a freestream density of 0.0001 kg/m^3. For a 1/100th scale model, binary scaling dictates that the density in the wind-tunnel test section would be 0.01 kg/m^3. Assuming a test flow area of 1 m^2 in the cross section, the power (given by the mass flow rate × area × velocity = $\rho U^3 A$) is then 3.4 GW, or an energy flux of 3.4 GW/m^2. To get an appreciation of the magnitude of this, let us compare it with the energy flux at the surface of the sun. The power output by the sun, or solar luminosity (L_{sun}), is known to be 3.9×10^{26} W. The solar power per unit area at a distance from the sun is given by the total power divided by the surface area of the sphere ($4\pi r^2$), with its radius being the distance from the sun's center. At the sun's surface, the radius is 7×10^5 km, yielding an energy flux of 0.064 GW/m^2. Compared to this value, the wind-tunnel power is about 53 times that of the sun's surface. Clearly, this power cannot be sustained for a long time. In addition, the stagnation temperature of the test gas for the reentry velocity reaches about 10,000 K, or approximately twice the surface temperature of the sun (~5,800 K), which is beyond the melting temperature of all known materials. Therefore, the only practical way to achieve hypersonic test conditions is to use short-duration facilities and to rely on thermal inertia to avoid melting the facility.

The use of shock waves to rapidly heat the test gas is currently the main ground testing technique for generating high enthalpy flows. Shock-heated test facilities are a class of wind tunnels that allow the duplication of flight velocities and high-temperature real-gas effects. Two types of such facilities are the reflected-shock tunnel (RST) and the shock-expansion tube or tunnel (SET). Both will be the main subjects of this book. These facilities, whether they are RSTs or SETs, are derived from extremely powerful shock tubes. These are short-duration facilities and are therefore known variously as pulse, impulse, or simply shock-tunnel facilities.

Because of the short-duration nature of the hypersonic test process, an important issue is whether there is sufficient test time. A requirement is that the pulse facilities must have sufficient time to fully establish steady-state flow over the test model. The most pertinent measure of test time is the ratio of the test "slug length" to the characteristic length of the flow process. As shown in Figure 1.2, the slug length ($L_{\text{slug}} = U \times t$) is the distance traveled by the volume of test gas during the period of steady test time, where U is the flow velocity and t is the test time. The characteristic length L may be represented by the model length if the flow is attached, or it includes the length of the separated zone for separated flow. Different estimates of test time requirements are used in the hypersonic testing community, depending on the nature of the flow process and the shape and orientation of the test model. Some reasonable rules of thumb for testing relatively slender external flow models are as follows:

https://doi.org/10.1017/9781009030991.002 Published online by Cambridge University Press

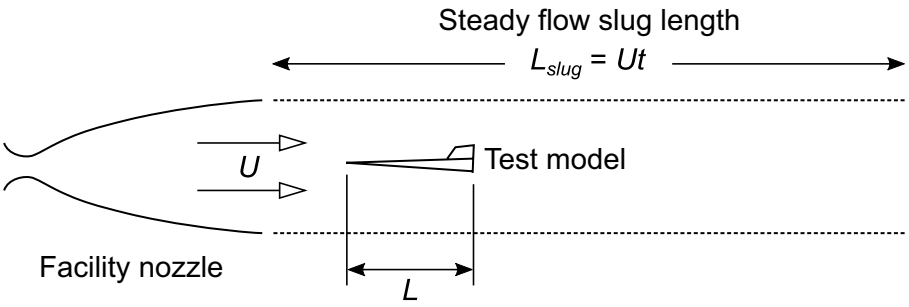

Figure 1.2 Slug length and characteristic length in the wind-tunnel test section.

$$\frac{Ut}{L} > 2, \quad \text{attached turbulent flow,} \tag{1.19}$$

$$\frac{Ut}{L} > 3, \quad \text{attached laminar flow,} \tag{1.20}$$

$$\frac{Ut}{L} > 10, \quad \text{separated flow.} \tag{1.21}$$

For testing streamline-shaped scramjet engines, it is a common practice to require a test slug of at least three model lengths in pulse facilities. Consider the testing of a 1-m long model. At Mach 10, the velocity is approximately 2,970 m/s (assuming a flight ambient temperature of 220 K). A 3-m gas slug would correspond to a test duration of 1 ms, which is readily achievable in RSTs. Similarly, at Mach 25, the velocity is 7,425 m/s. A 3-m slug length would correspond to a test period of 0.4 ms. The enthalpy level and the test time can be reached in SETs.

There are other considerations associated with RSTs and SETs, such as test gas contamination, which may be due to test gas dissociation in the test facilities, and the contamination of the test gas by the driver gas. Test gas dissociation is a consequence of the extremely high temperature encountered in the shock-heated gas in the facilities, which is especially a problem in the reflected-shock region in RSTs. This may also be an issue in SETs, but to a lesser degree. Driver gas contamination is related to the premature leakage of the gas medium used to drive the pulse facility which only affects RSTs.

1.4.2 Arc-jets

Because of the extremely short-duration nature of shock-tunnel facilities, intermittent flow facilities have also been used for hypersonic testing. At the lower boundary of hypersonic flow, such as at about Mach 7, these facilities can meet the requirements of most of the simulation parameters. However, at higher Mach numbers, they generally cannot meet the key simulation parameters, such as binary scaling.

The most common intermittent flow test facilities are arc-jets that have much longer run times (typically tens of minutes) than are available in pulse facilities. There are

https://doi.org/10.1017/9781009030991.002 Published online by Cambridge University Press

different types of arc-jet wind tunnels, but they all utilize electric discharge for heating the test medium to extremely high temperatures prior to expanding it in a nozzle to the test section (Smith et al. 2002). Arc-heaters can generate test flow total enthalpies of more than 30 MJ/kg or temperatures of the order of 10,000 K. On the other hand, the pressure in the arc-settling chamber, and thus the test flow stagnation pressure, is limited to about 100 atm. There is also a limit on the product of pressure and enthalpy an electric arc can achieve so that the maximum enthalpy is obtained at low pressures (Park 1995, 1996b). In contrast, RSTs can generate test flow stagnation pressures of about 1,000 atm. and SETs can reach even higher. Another metric to consider is the power level attained in the test facility. Arc-jets consume less than 150 MW of electrical power. Compared to the GW level delivered in large pulse facilities (as discussed in Section 1.4.1), arc-jets cannot be expected to be as capable as shock tunnels in providing hypersonic test conditions.

Arc-jets also suffer from metallic erosion from the electrodes. And since very high temperatures are generated in the gas ionized by the arc, significant amount of test-medium dissociation are formed in the plenum, just as in the case of RSTs, making the issues of chemical dissociation and contamination more severe. And although arc-jets provide a longer test duration, the test flows can be unstable and nonuniform. Because of the above reasons, arc-jets are not suitable for accurate aerothermodynamic and combustion experiments in the hypervelocity regime. However, arc-jets have indeed played a significant role in testing air-breathing propulsion in the lower hypersonic range, as demonstrated by the testing of the Hyper-X engine at the Mach 7 condition in NASA Langley's Arc-Heated Scramjet Test Facility (Guy et al. 1996, Voland et al. 1998).

Due to its relatively long test duration, arc-jets have been used extensively for testing thermal protection systems to assess materials' response and structural survival in reentry vehicles. For this reason, arc-jet wind tunnels are also referred to as aerothermal test facilities. But since arc-jets have lower total pressure capabilities than pulse facilities, they generally cannot satisfy binary scaling and Reynolds number requirements at the hypervelocity regime. Because of this, they will not be included in this book.

There are, indeed, other types of ground testing facilities to generate hypersonic flow conditions, such as those discussed in Chinitz et al. (1994) and in the book edited by Lu and Marren (2002). These facilities have different capabilities, advantages, and disadvantages, and are in different stages of readiness. Currently, shock-heated pulse facilities are the best option and the most widely used techniques for testing in the hypersonic regime. Therefore, they are selected as the focus of this book.

1.5 Outline of the Book

The purpose of the book is to present and discuss the theories and techniques for hypervelocity ground testing facilities. As the attention here is on shock-heated high-enthalpy pulse facilities, the fundamental theory of shock waves and its application to generate high-enthalpy flows in shock tunnels are presented in Chapter 2.

https://doi.org/10.1017/9781009030991.002 Published online by Cambridge University Press

Shock-wave-heated facilities can be driven in a number of ways. The book then examines the different driver techniques that have been developed. These include the heated light-gas, free-piston, and detonation drivers, presented in Chapters 3–5. The theory of operation of these drivers and their applications in hypersonic testing are also discussed.

The development of long-duration shock tunnels is of particular interest to the hypersonic community as it can overcome the stringent limitation of test time. The concepts involved and the accomplishments in actual facilities are presented in Chapter 6.

The facility nozzle is a critical component in high-enthalpy shock tunnels, as it controls the quality of the flow delivered to the test section. Chapter 7 examines various methods for designing hypersonic flow nozzles, including conventional method of characteristics as well as the state-of-the-art CFD-based design approaches.

The book ends by discussing the phenomena associated with high-enthalpy flows, how they are manifested in real flight, and how they are studied in ground test facilities. Chapter 8 includes the experimental methods for measuring aerodynamic forces and moments, aerothermal heating, boundary-layer transition, as well as a discussion of supersonic combustion and scramjet testing.

Nomenclature

a	sound speed
A_{capture}	inlet capture area
c_p	specific heat capacity at constant pressure
Da_1	Damköhler's first number
Da_2	Damköhler's second number
E	total energy emitted
F	thrust
h	enthalpy
L	length
L_{slug}	slug length
$\dot{m}_{\text{air}}$	mass flow rate of air
M	Mach number
p	pressure
q_{conv}	convective heat transfer rate
q_{rad}	radiative heat transfer rate
R	gas constant
R_N	nose radius
Re	Reynolds number
t	time
T	temperature
U	velocity
U_{exhaust}	engine exhaust velocity

https://doi.org/10.1017/9781009030991.002 Published online by Cambridge University Press

β	local shock-wave angle
δ	boundary-layer thickness
γ	ratio of specific heats

Subscripts:

s	post-shock condition
t	total or stagnation condition
∞	freestream condition

References

Abbany, Z. (2021). NASA Rover Attempting Most Difficult Martian Touchdown. *Deutsche Welle*, February 18. https://bit.ly/3rM214C (Accessed: February 28, 2021).

Aharonson, O., Russell, C. T., Head, J. W. III, et al. (2020). The Science Mission of SpaceIL's Beresheet Lander: Plans and Results. *51st Lunar and Planetary Science Conference*, Woodlands, Texas, 1267.

Allen, H. J. and Eggers, A. J. (1953). A Study of the Motion and Aerodynamic Heating of Ballistic Missiles Entering the Earth's Atmosphere at High Supersonic Speeds. *NACA-RM-A53D28*. https://ntrs.nasa.gov/citations/20050019430 (Accessed: May 2, 2023).

Allen, H. J. and Eggers, A. J. (1958). A Study of the Motion and Aerodynamic Heating of Ballistic Missiles Entering the Earth's Atmosphere at High Supersonic Speeds. *NACA-TR-1381*. (Supersedes NACA-TN-4017 by the same authors, 1957). https://history.arc.nasa.gov/hist_pdfs/awards/hjaa_1970a.pdf (Accessed: May 2, 2023).

Anderson, G., Kumar, A., and Erdos, J. (1990). Progress in Combustion Technology with Computation and Experiment. *AIAA Paper 90-5254*.

Anderson, J. D. Jr. (2006). *Hypersonic and High-Temperature Gas Dynamics*, 2nd ed. Reston, VA: AIAA.

Anon. (1980). *Aerodynamic Design Data Book – Orbiter Vehicle*, Vol. 1, Rockwell International, Space Division. *SD72-SH-0060-1M*.

Arney, D. (2016). Reusable Vehicles Come to Forefront. *Aerospace America*, AIAA, December, **54**(11), 70.

Barbosa, R. C. (2013). China's Chang'e-3 and Jade Rabbit Duo Land on the Moon. *Nasaspaceflight.com*, December 14. https://bit.ly/3lenwbO (Accessed: February 27, 2021).

Berry, S. A., Kimmel, R., and Reshotko, E. (2011). Recommendations for Hypersonic Boundary Layer Transition Flight Testing. *AIAA Paper 2011-3415*.

Bertin, J. J. (1994). *Hypersonic Aerothermodynamics*. Washington, DC: AIAA, pp. 231–276.

Bertin, J. J. and Cummings, R. M. (2006). Critical Hypersonic Aerothermodynamic Phenomena. *Annual Review of Fluid Mechanics*, **38**, 129–157.

Brauckmann, G. J., Paulson, J. W. Jr., and Weilmuenster, K. J. (1995). Experimental and Computational Analysis of Shuttle Orbiter Hypersonic Trim Anomaly. *Journal of Spacecraft and Rockets*, **32**(5), 758–764.

Button, K. (2018). Hypersonic Weapons Race. *Aerospace America*, AIAA, June, **56**(6), 20–25.

https://doi.org/10.1017/9781009030991.002 Published online by Cambridge University Press

Charters, A. C. and Thomas, R. N. (1945). The Aerodynamic Performance of Small Spheres from Subsonic to High Supersonic Velocities. *Journal of the Aeronautical Sciences*, **12**(4), 468–476.

Chen, F.-J. and Berry, S. A. (2010). HyBoLT Flight Experiment. *NASA Technical Memorandum*, NASA/TM-2010-216725.

Chinitz, W., Erdos, J. I., Rizkalia, O., Anderson, G. Y., and Bushnell, D. M. (1994). Facility Opportunities and Associated Stream Chemistry Considerations for Hypersonic Air-Breathing Propulsion. *Journal of Propulsion and Power*, **10**(1), 6–17.

Costa, M., Pérez, M., Almeida, M., et al. (2016). Rosetta: Rapid Science Operations for a Dynamic Comet. *AIAA Paper* 2016–2538.

Cox, R. N. and Crabtree, L. F. (1965). *Elements of Hypersonic Aerodynamics*. New York: Academic Press.

Crowder, R. S. and Moot, J. D. (1965). Apollo Entry Aerodynamics, *Journal of Spacecraft and Rockets*, **6**(3), 302–307.

Desai, P. N., Lyons, D. T., Tooley, J., and Kangas, J. (2006). Entry, Descent, and Landing Operations Analysis for the Stardust Re-Entry Capsule. *AIAA Paper* 2006–6410.

Edney, B. E. (1968a). Anomalous Heat Transfer and Pressure Distributions on Bunt Bodies at Hypersonic Speeds in the Presence of an Impinging Shock. *FFA Report* 115, Flygtekniska Försöksanstalten (The Aeronautical Research Institute of Sweden), Stockholm.

Edney, B. E. (1968b). Effects of Shock Impingement on the Heat Transfer around Blunt Bodies. *AIAA Journal*, **6**(1),15–21.

eoPortal Chang'e-5. (n.d.). Chang'e-5 (China's Lunar Sample Return Mission)/CE-5. https://bit.ly/3lesd5g (Accessed: March 2, 2021).

eoPortal Hayabusa-2. (n.d.). Hayabusa-2, Japan's Second Asteroid Sample Return Mission. https://bit.ly/3lcw1nE (Accessed: March 2, 2021).

Fay, J. A. and Riddell, F. R. (1958). Theory of Stagnation Point Heat Transfer in Dissociated Air. *Journal of Aeronautical Sciences*, **25**(2), 73–85.

Francis, W. L. (1965). Experimental Heat-Transfer Study of Shock Impingement on Fins in Hypersonic Flow. *Journal of Spacecraft and Rockets*, **2**(4), 630–632.

Gibney, E. (2019). China Plans Mission to Earth's Pet Asteroid. *Nature*, April 30. www.nature.com/articles/d41586-019-01390-5 (Accessed: February 28, 2021).

Grinstead, J. H., Jenniskens, R., Cassell, A. M., Albers, J., and Winter, M. W. (2011). Airborne Observation of the Hayabusa Sample Return Capsule Re-entry. *AIAA Paper* 2011–3329.

Guy, R. W., Rogers, R. C., Puster, R. L., Rock, K. E., and Diskin, G. S. (1996). The NASA – Langley Scramjet Test Complex. *AIAA Paper* 96–3243.

Hadhazy, A. (2017). Space Station Experiment Targets Parkinson's. *Aerospace America*, AIAA, September, **55**(8), 9.

Hadhazy, A. (2019). Lunar Far Side Comes into Focus. *Aerospace America*, AIAA, April, **57**(4), 31–34.

Hiers, R. S. and Loubsky, W. J. (1967). Effects of Shock-Wave Impingement on the Heat Transfer on a Cylindrical Leading Edge. *NASA TN D-3859*.

Hodges, A. J. (1957). The Drag Coefficient of Very High Velocity Spheres, *Journal of the Aeronautical Sciences*, **24**(10), 755–758.

Hofactor, C. (2020a). How to Make a Megaconstellation. *Aerospace America*, AIAA, March, **58**(3), 16–23

Hofactor, C. (2020b). One of These Companies Could Deliver American Astronauts to the Moon in 2024. *Aerospace America*, AIAA, April 30. https://bit.ly/3qGqAyF (Accessed: February 27, 2021).

JAXA. (2019). Shooting bullets into Ryugu! *JAXA*, February 18. https://bit.ly/3bJVaDa (Accessed: February 27, 2021).

Justus, C. G. and Braun, R. D. (2007). Atmospheric Environments for Entry, Descent and Landing (EDL). In *5th International Planetary Probes Workshop and Short Course*, 23–29 June, Bordeaux, France.

Klotz, I. (2017). Recycling Rockets. *Aerospace America*, AIAA, September, **55**(8), 32–39.

Koppenwallner, G. (1987). Low Reynolds Number Influence on Aerodynamic Performance of Hypersonic Lifting Vehicles, Paper 11. *AGARD Conference Proceedings No. 428*, Aerodynamics of Hypersonic Lifting Vehicles, November.

Lauretta, D. S., Balram-Knutson, S. S., Beshore, E., et al. (2017). OSIRIS-REx: Sample Return from Asteroid (101955) Bennu. *Space Science Reviews*, **212**, 925–984.

Lebreton, J.-P. and Matson, D. L. (2002). The Huygens Probe: Science, Payload and Mission Overview. *Space Science Reviews*, **104**, 59–100.

Lebreton, J.-P., Witasse, O., Sollazzo, C., et al. (2005). An Overview of the Descent and Landing of the Huygens Probe on Titan. *Nature*, **438**(8), 758–764.

Lu, F. K. and Marren, D. E. (eds.) (2002). *Advanced Hypersonic Test Facilities*. AIAA Progress in Astronautics and Aeronautics, Vol. 198. Reston, VA: AIAA.

Maise, G., Powell, J., Paniagua, J., et al. (2003). Application of the MITEE Nuclear Ramjet for Ultra Long Range Flyer Missions in the Atmospheres of Jupiter and Other Giant Planets. *Paper IAC-03-Q.4.09*, *54th International Astronautical Congress*, Bremen, Germany, September–October.

Malik, T. (2012). Death of DARPA's Superfast Hypersonic Glider Explained. *Space.com*, April 23. https://bit.ly/3lgwepV (Accessed: March 2, 2021).

Martos, J. F. d. A., Rêgo, I. d. S., Laiton, S. N. P., et al. (2017). Experimental Investigation of Brazilian 14-X B Hypersonic Scramjet Aerospace Vehicle. *International Journal of Aerospace Engineering*, 2017. Article ID 5496527. https://doi.org/10.1155/2017/5496527 (Accessed: May 2, 2023).

Marvin, J. G. and Deiwert, G. S. (1965). Convective Heat Transfer in Planetary Gases, *NASA Technical Report TR R-224*.

Maus, J. R., Griffith, B. J., Szema, K. Y., and Best, J. T. (1984). Hypersonic Mach Number and Real Gas Effects on Space Shuttle Orbiter Aerodynamics, *Journal of Spacecraft and Rockets*, **21**(2), 136–141.

McBride, B. J. and Gordon, S. (1996). Computer Program for calculation of Complex Chemical Equilibrium Compositions and Applications. II. Users Manual and Program Description. *NASA Reference Publication RP-1311*.

McCurdy, H. E. (2005). Low-Cost Innovation in Spaceflight. The Near Earth Asteroid Rendezvous (NEAR) Shoemaker Mission. *Monographs in Aerospace History*, **36**, NASA SP-2005-4536.

NASA. (2009). NASA and ISRO Satellites Perform in Tandem to Search for Ice on the Moon, August 20. www.nasa.gov/mission_pages/Mini-RF/news/tandem_search.html (Accessed: February 27, 2021).

NASA. (2020). NASA's OSIRIS-REx Successfully Stows Sample of Asteroid Bennu. *NASA News Release*, October 29. https://go.nasa.gov/3cojZng (Accessed: February 28, 2021).

NASA Mars. (2021). *Mars 2020 Perseverance Rover*. https://mars.nasa.gov/mars2020/ (Accessed: February 28, 2021).

NASA Perseverance. (2020). Mars 2020/Perseverance. *NASA Fact Sheet*. https://mars.nasa.gov/files/mars2020/Mars2020_Fact_Sheet.pdf (Accessed: February 28, 2021).

Newlander, R. A. (1961). Effect of Shock Impingement on the Distributions of Heat-Transfer Coefficients on a Right Circular Cylinder at Mach Numbers of 2.65, 3.51, and 4.44. *NASA TN D-642*.

Norris, G. (2013). Skunk Works Reveals SR-71 Successor Plan. *Aviation Week and Space Technology*, November 1. https://bit.ly/40VCJSv (Accessed: May 1, 2023).

Odom, T. and Johnston, D. (2018). Exploring High-Speed Propulsion for Weapons, Passenger Aircraft. *Aerospace America*, AIAA, December, **56**(11), 49.

Oswatitsch, K. (1951). Ähnlichkeitsgesetz für Hyperschallströmung (Similarity Laws for Hypersonic Flow). *Zeitschrift für Angewandte Mathematik und Physik ZAMP (Journal of Applied Mathematics and Physics)*, **2**(4), 249–264.

Oswatitsch, K. (1980). Similarity Laws for Hypersonic Flow. In *Contributions to the Development of Gas Dynamics*, ed. W. Schneider and M. Platzer. Braunschweig: Vieweg Verlag, pp. 76–88.

Owen, T., Raulin, F., McKay, C., et al. (1997). The Relevance of Titan and Cassini/Huygens to Pre-biotic Chemistry and the Origin of Life on Earth. In *Huygens: Science, Payload and Mission, ESA SP 1177*, ed. A. Wilson. Noordwijk: ESA Publications Division, ESTEC, pp. 231–233.

Park, C. (1995). Experimental Simulation and Evaluation of Chemical Effects. In *Aerothermochemistry for Hypersonic Technology, Lecture Series 1995–04*, ed. G. S. R. Sarma. Belgium: Von Karman Institute for Fluid Dynamics.

Park, C. (1996a). Experimental Evaluation of Real-Gas Phenomena in High-Enthalpy Impulse Test Facilities. *AIAA Paper 96–2234*.

Park, C. (1996b). Experimental Evaluation of Real-Gas Phenomena in High-Temperature Aerothermal Test Facilities: A Review. *AIAA Paper 96–2207*.

Planetary Society. (n.d.). *Tianwen-1 and Zhurong, China's Mars Orbiter and Rover*. www.planetary.org/space-missions/tianwen-1 (Accessed: May 1, 2023).

Ray, A. D. and Palko, R. L. (1965). An Investigation of the Effects of Shock Impingement on a Blunt Leading Edge. *AEDC-TR-65-153*. U.S. Air Force.

Schneider, S. P. (1999). Flight Data for Boundary-Layer Transition at Hypersonic and Supersonic Speeds. *Journal of Spacecraft and Rockets*, **36**(1), 8–20.

Sforza, P. M. (2012). *Theory of Aerospace Propulsion*. Waltham, MA: Elsevier, pp. 536–539.

Siddiqi, A. A. (2018). Beyond Earth: A Chronicle of Deep Space Exploration. *NASA SP-2018-4041*, NASA History Division.

Siler, L. G. and Deskins, H. E. (1964). Effect of Shock Impingement on Heat-Transfer and Pressure Distributions on a Cylindrical-Leading-Edge Model at Mach Number 19. *AEDC-TDR-64-228*, U.S. Air Force, November.

Singh, L., Sharma, S. P., and Moore, C. (2019). Space Exploration Focuses on Asteroids. *Aerospace America*, AIAA, December, **56** (11), 72.

Smith, D. M., Felderman, E. J., Shope, F. L., and Balboni, J. A. (2002). *Arc-Heated Facilities. In Advanced Hypersonic Test Facilities*, AIAA Progress in Astronautics and Aeronautics, Vol. 198. Reston, VA: AIAA, pp. 279–314.

SpaceX Falcon. (2021) *Falcon Heavy*. www.spacex.com/vehicles/falcon-heavy/ (Accessed: February 27, 2021).

Stevens, V. I. (1950). Hypersonic Research Facilities at the Ames Aeronautical Laboratory, *Journal of Applied Physics*, **21**(11), 1150–1155.

Sutton, K. and Graves, R. A. Jr. (1971). A General Stagnation-Point Convective-Heating Equation for Arbitrary Gas Mixtures, *NASA Technical Report TR R-376*.

Tauber, M. E. (1989). A Review of High-Speed, Convective, Heat-Transfer Computational Methods, *NASA Technical Paper 2914*.

Tauber, M. E., Meneses, G. P., and Adelman, H. G. (1987). Aerothermodynamics of Transatmospheric Vehicles. *Journal of Aircraft*, **24**(9), 594–602.

The Hindu. (2009). Chandrayaan Confirms Moon Was once Completely Molten: Scientist. *The Hindu*. https://bit.ly/41OO7R3 (Accessed: May 1, 2023).

Urzay, J. (2018). Supersonic Combustion in Air-Breathing Propulsion Systems for Hypersonic Flight. *Annual Review of Fluid Mechanics*, **50**, 593–627.

Voland, R. T., Rock, K. E., Huebner, L. D., et al. (1998). Hyper-X Engine Design and Ground Test Program. *AIAA Paper 98–1532*.

Watts, J. D. (1968). Flight Experience with Shock Impingement and Interference Heating on the X-15-2 Research Airplane, *NASA Technical Memorandum*, NASA/TM X-1669.

Wood, P. and Cliff, R. (2020). *A Case Study of the PRC's Hypersonic Systems Development*. E-book. China Aerospace Studies Institute, Air University, September 20. https://bit.ly/38B1MSm (Accessed: March 2, 2021).

Wright, R. L. and Zoby, E. V. (1977). Flight Boundary Layer Transition Measurements on a Slender Cone at Mach 20. *AIAA Paper 77–719*.